

Intra-operative Brain Shift Estimation Using Atlas of Brain Deformations and Constrained Kalman Filter

Mehran Shakarami, Amir Abolfazl Suratgar, *Senior Member, IEEE*, and Heidar Ali Talebi, *Senior Member, IEEE*

Abstract—Intra-operative brain shift decreases the accuracy of neuronavigation systems based on pre-operative images. In this paper, this problem is addressed by calculating an estimation of brain shift which can be employed to update the pre-operative brain images. Therefore, the precision of navigation can be improved. In this regard, a brain shift estimation method is proposed using an Atlas of brain deformations and Constrained Kalman Filter (ACKF). In addition, it is proved that the obtained ACKF estimation is the best unbiased minimax estimation when the risk function is the estimation error variance. Furthermore, a comparison is performed between ACKF and two existing methods, namely Constrained Kalman Filter (CKF) and atlas-based method. The comparison demonstrates that ACKF results in a more accurate estimation and needs less computation time. Finally, the supremacy of the proposed ACKF method with respect to CKF and atlas-based method is illustrated through simulation.

Index Terms—Brain shift, image guided neurosurgery, constrained Kalman filter, atlas-based method, finite element method.

I. INTRODUCTION

Image Guided Neurosurgery (IGNS) systems are employed in neurosurgery and help surgeons in surgical visualization and navigation. Hence surgeons can remove tumors without damaging healthy brain tissues surrounding them. Most of IGNS systems only utilize pre-operative images like pre-operative MRI (pMRI) or pre-operative CT (pCT). However, due to many factors, like tumor resection, gravity, edema, pharmacologic responses, and drainage of cerebrospinal fluid (CSF), the brain deforms during surgery. This brain deformation is known as “brain shift” and degrades the accuracy of IGNS systems [1], [2], [3].

In order to compensate brain shift, two main candidates are intra-operative medical imaging and computational model-based techniques. The first method includes intra-operative MRI (iMRI) [4], intra-operative CT (iCT) [5], and intra-operative Ultrasound (iUS) [6]. iMRI is cumbersome and expensive, and iCT is not very attractive due to high doses of radiation. While iUS provides real-time images and is much more cheaper than iMRI and iCT, its resulting images suffer from the lack of image clarity and have lower soft tissue contrast. In the second approach, biomechanical models of the brain are employed to improve pre-operative images. Towards

this end, the solutions of model are driven for some boundary conditions and utilized to deform pre-operative images to their current position. Two challenges of this approach are that the boundary conditions in the operating room are unknown, and computational time associated with estimation techniques should meet the real-time constraints of neurosurgery. To overcome the first challenge, sparse intra-operative information obtained by imaging the exposed brain surface are employed in [7], [8], [9], [10]. In [7], the estimation of brain shift is obtained using a sparse extrapolative technique. The brain model is derived by cortical surface deformations obtained from laser range scanner in [8], [9]. In [10], the boundary conditions are obtained from data of laser range scanner and the brain model is solved by the extended finite element method. The second challenge is considered in [11], [12], [13] and is addressed by employing adaptive dynamic relaxation method [11], atlas of brain deformations [12], and iterative methods [13].

In addition to sparse intra-operative data, it is proposed in [12] to utilize a series of pre-operative computed brain deformations for obtaining a more accurate estimation with less computational cost. This method, known as atlas-based method, has two steps: first, an “atlas” of brain deformations, which is a collection of brain deformations based on possible boundary conditions in the operating room, is computed pre-operatively; then, the atlas is matched intra-operatively with the sparse data using a constrained linear inverse model. The matching method between the atlas and sparse data is improved in [14], [15], and is employed in [16] to develop an automated process for near real-time brain shift estimation. In order to investigate the method using experimental data, an evaluation in clinical cases is performed in [17] that has shown encouraging results.

A powerful tool for solving estimation problems is Kalman filter, and it has been shown that this technique yields promising results in a wide variety of applications, such as state estimation of power systems [18], control of microgrippers [19], etc. An extension of the Kalman filter, constrained Kalman filter, results in a more accurate estimation when there exist linear equality constraints on the variables [20], and it is utilized for solving different estimation problems in [21], [13]. A method for localization of autonomous underwater vehicles in the presence of unknown ocean currents is presented in [21]. In our previous work [13], sparse intra-operative data is employed together with the Constrained Kalman Filter (CKF) to estimate boundary conditions of the brain model. Then,

The authors are with the Center of Excellence on Control and Robotics, Department of Electrical Engineering, Amirkabir University of Technology (Tehran Polytechnic), Tehran 15914, Iran (e-mail: mehran.shakarami@aut.ac.ir; a-suratgar@aut.ac.ir; alit@aut.ac.ir).

to improve the computational time of estimation, a recursive method is proposed.

The main contribution of this paper is to estimate brain shift by combining the information of an Atlas of brain deformations and Constrained Kalman Filter (ACKF). The proposed ACKF method employs sparse intra-operative measurement of the exposed brain surface and a biomechanical model of brain to estimate brain shift. It is shown that the resulting estimation is the best minimax estimation when the covariance of boundary conditions of the model is unknown. Then, ACKF is compared with two existing methods, one of which uses the same computing method, i.e. CKF, and the other uses the same information sources, i.e. the atlas-based method, and it is demonstrated that ACKF results in a more accurate estimation. In addition to accuracy, ACKF inherently has a lower computational cost. Simulation results are also presented by using finite element method to verify the claims.

II. MATERIALS AND METHODS

Biot's consolidation theory is originally developed to represent biphasic soil consolidation [22], and is utilized in [23] as the governing equations of brain. In the next section, this model which is selected as the model of brain is introduced; afterwards, the proposed estimation method and its properties are stated.

A. Biomechanical Model

The biphasic model obtained from Biot's consolidation theory assumes the continuum as a porous solid tissue matrix infused with an interstitial fluid. Two sets of equations, equations of linear elasticity for the solid matrix and Darcy's law for the fluid pressure, are coupled to build this model as [24]:

$$\nabla \cdot G \nabla \mathbf{u} + \nabla \frac{G}{1-2\nu} (\nabla \cdot \mathbf{u}) - a \nabla p = (\rho_t - \rho_f) \mathbf{g} \quad (1a)$$

$$a \frac{\partial}{\partial t} (\nabla \cdot \mathbf{u}) + \frac{1}{S} \frac{\partial p}{\partial t} - \nabla \cdot k \nabla p = \Psi \quad (1b)$$

where \mathbf{u} and p are the displacement vector and interstitial pressure to be computed, and other material properties are summarized in Table I [12]. Mechanical equilibrium is expressed by (1a), and it is dependent on surface forces and displacements, interstitial fluid pressure gradient, and changes in tissue buoyancy forces. The buoyancy forces, which counteract gravitational forces, intra-operatively reduce due to CSF drainage. As a result, the brain deforms, and this effect is expressed on the right-hand side of (1a) [25]. The relationship between the time rate of change of volumetric strain and fluid pressure is also presented by (1b). For the brain, it is always assumed that the interstitial fluid is incompressible and saturates the tissue; therefore, the terms a and $1/S$ are taken equal to one and zero, respectively [12].

Model (1) explains the time-evolution of \mathbf{u} and p . However, the brain tissues are stationary when sparse intra-operative information is obtained. In other words, linear elastic mechanical behavior of the brain is important in brain shift estimation problem [26], [27]. Therefore, the steady state form of (1)

TABLE I: Parameters used in the biphasic model.

Parameter	Description	Value
G	Shear modulus	724 Pa
ν	Poisson's ratio	0.45
a	Ratio of fluid volume extracted to change in solid volume	1
ρ_t	Tissue density	1000 kg/m ³
ρ_f	Fluid density	1000 kg/m ³
$\frac{1}{S}$	Fluid that can be forced into the tissue under constant volume	0
k	Hydraulic conductivity	1×10^{-10} m ³ /s/kg
Ψ	Pressure source strength	0 Pa/s

needs to be considered for estimating brain shift, and it can be solved numerically by employing the Galerkin's finite element method (FEM) to get

$$\mathbf{K} \mathbf{x} = \mathbf{b} \quad (2)$$

where $\mathbf{K} \in \mathbb{R}^{n \times n}$ is the stiffness matrix that contains the geometric and material behavior, $\mathbf{x} \in \mathbb{R}^n$ represents discrete values of \mathbf{u} and p at FEM mesh nodes, and $\mathbf{b} \in \mathbb{R}^n$ includes boundary condition information which is unknown in the operating room [23], [27]. Furthermore, n is the total number of degrees of freedom in the entire domain and is equal to the number of variables, 3 displacements and one pressure, multiplied by the number of nodes. It is worth to mention that \mathbf{K} is a full rank matrix which is a consequence of employing a valid FEM and proper boundary conditions [28].

B. Estimation Method

In order to estimate brain shift, two sources of information, sparse intra-operative measurement of the exposed brain surface and a pre-operative atlas of brain deformations, are utilized in this paper. The sparse intra-operative data, $\mathbf{y} \in \mathbb{R}^m$, is related to \mathbf{x} by a full row rank matrix $\mathbf{C} \in \mathbb{R}^{m \times n}$ as follows [29]:

$$\mathbf{y} = \mathbf{C} \mathbf{x}. \quad (3)$$

To construct the atlas, possible boundary conditions in the operating room are utilized pre-operatively to compute the solutions of brain model. Then, the obtained pre-operative solutions are assembled in a matrix $\mathbf{M} \in \mathbb{R}^{n \times l}$ (the atlas) where l is the number of solutions. In other words, the i th column of \mathbf{M} is the solution of (1) for the i th boundary condition. Intra-operative brain shift is considered as a linear combination of the computed solutions as [12]:

$$\mathbf{x} = \mathbf{M} \boldsymbol{\alpha} \quad (4)$$

where $\boldsymbol{\alpha} \in \mathbb{R}^l$ is the unknown vector of regression coefficients.

To estimate brain shift, the vector \mathbf{b} is considered as a Gaussian random vector with known mean vector $\bar{\mathbf{b}}$ and unknown covariance matrix [13]. This assumption is valid because \mathbf{b} includes the applied forces to the brain which can be considered as random signals, and by using (2) and (4), one can conclude that \mathbf{x} and $\boldsymbol{\alpha}$ are also random vectors. Therefore, the relationships between the mean vector of \mathbf{x} , $\bar{\mathbf{x}}$, the mean vector of $\boldsymbol{\alpha}$, $\bar{\boldsymbol{\alpha}}$, and $\bar{\mathbf{b}}$ are as follows:

$$\begin{aligned} \bar{\mathbf{x}} &= \mathbf{M} \bar{\boldsymbol{\alpha}} \\ \bar{\mathbf{b}} &= \mathbf{K} \mathbf{M} \bar{\boldsymbol{\alpha}}. \end{aligned} \quad (5)$$

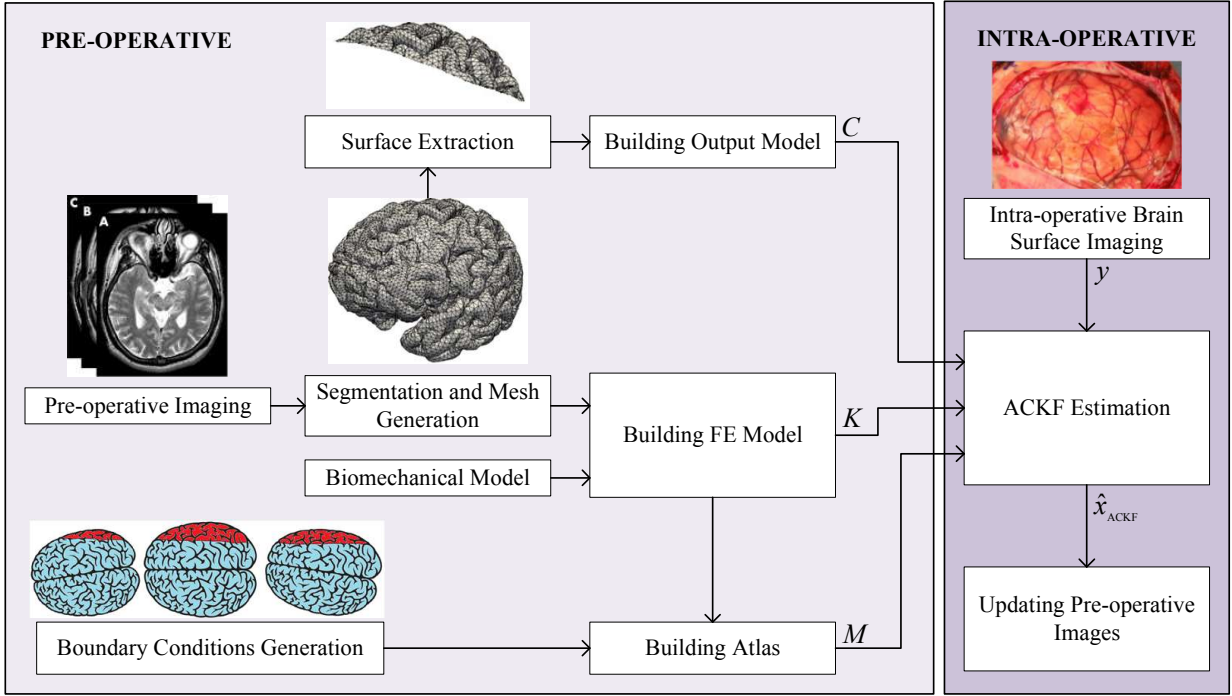


Fig. 1: Overall procedure for brain shift compensation.

Since the boundary conditions are unknown in brain shift estimation problem, it is reasonable to estimate \hat{b} , which includes the boundary conditions, and then calculate x . By considering this approach known as inverse method, the estimation of b , \hat{b} , can be considered as follows:

$$\arg \min_{\hat{b}} E[(b - \hat{b})^T (b - \hat{b})]. \quad (6)$$

To use the atlas, (2) and (4) should be substituted in (6) which results in

$$\arg \min_{\hat{\alpha}} E[(KM\alpha - KM\hat{\alpha})^T (KM\alpha - KM\hat{\alpha})] \quad (7)$$

where $\hat{\alpha}$ is the estimation of α . In addition to (7), the resulting estimation should satisfy (3). Therefore, $\hat{\alpha}$ can be obtained from the following constrained optimization problem

$$\begin{aligned} \arg \min_{\hat{\alpha}} \quad & E[(KM\alpha - KM\hat{\alpha})^T (KM\alpha - KM\hat{\alpha})] \\ \text{subject to} \quad & y = CM\hat{\alpha}. \end{aligned}$$

To find the solution of optimization problem, one needs to consider the Lagrangian of the constrained problem as follows:

$$L = E[(KM\alpha - KM\hat{\alpha})^T (KM\alpha - KM\hat{\alpha}) + 2\lambda^T (y - CM\hat{\alpha})]. \quad (8)$$

where $\lambda \in \mathbb{R}^m$ is the Lagrange multiplier vector. Let the probability density function of α be $f(\alpha)$, then we can rewrite L as:

$$\begin{aligned} L = \int_{-\infty}^{\infty} \alpha^T F \alpha f(\alpha) d\alpha - 2\hat{\alpha}^T F \int_{-\infty}^{\infty} \alpha f(\alpha) d\alpha \\ + \hat{\alpha}^T F \hat{\alpha} \int_{-\infty}^{\infty} f(\alpha) d\alpha + 2\lambda^T (y - CM\hat{\alpha}) \end{aligned}$$

where

$$F := M^T K^T K M. \quad (9)$$

Noting that the second and third integrals are equal to $\bar{\alpha}$ and one respectively, $\hat{\alpha}$ should satisfy the following equations

$$\begin{aligned} \frac{\partial L}{\partial \hat{\alpha}} &= -2F\bar{\alpha} + 2F\hat{\alpha} - 2M^T C^T \lambda = 0 \\ \frac{\partial L}{\partial \lambda} &= 2(y - CM\hat{\alpha}) = 0. \end{aligned}$$

Solving these equations for λ and $\hat{\alpha}$ results in

$$\begin{aligned} \lambda &= (CMF^{-1}M^T C^T)^{-1} (y - CM\bar{\alpha}) \\ \hat{\alpha} &= \bar{\alpha} + F^{-1}M^T C^T (CMF^{-1}M^T C^T)^{-1} (y - CM\bar{\alpha}). \end{aligned} \quad (10)$$

By utilizing the obtained $\hat{\alpha}$ from (10) and (9), ACKF estimation \hat{x}_{ACKF} can be found from (4) and (5) as follows:

$$\begin{aligned} \hat{x}_{ACKF} &= \bar{x} + M (M^T K^T K M)^{-1} M^T C^T \\ &\quad \times (CM (M^T K^T K M)^{-1} M^T C^T)^{-1} (y - C\bar{x}). \end{aligned} \quad (11)$$

It should be mentioned that for obtaining \bar{x} , either it can be chosen equal to zero or some information regarding the boundary conditions in the operating room can be used intra-operatively. For example, one can assume that the gravity and CSF drainage are the reasons for \bar{x} [13]. Note that in the operating room, an approximation of this information can be provided by the surgeon, and the calculation of \bar{x} does not take much time since the brain model needs to be solved only once. On the other hand, for the solution exists, the number of pre-operative estimations of brain shift, l , should be $m \leq l \leq n$, and the matrix M should be full column rank. In other words, the utilized boundary conditions for constructing

the atlas should be linearly independent. However, if this condition is not satisfied, the employed boundary conditions can be modified or the Tikhonov regularization method [30] can be used to obtain an approximation of ACKF estimation.

A schematic of pre- and intra-operative steps for brain shift compensation using ACKF estimation is shown in Figure 1. Pre-operative brain images are usually captured one day or more before surgery and utilized for constructing a patient-specific FE model [8]. Based on pre-operative planning, approximate head orientation and craniotomy size are obtained and used for building the output model (3). Moreover, possible conditions in the operating room are employed for generating different boundary conditions; and the solutions of FE model for these boundary conditions build the atlas [12]. Intra-operatively, images of exposed brain surface are acquired and used with the FE modal and the atlas for estimating brain shift. Then, the pre-operative images are updated using the obtained estimation to improve their accuracy. It is worth noting that most time intensive steps are performed pre-operatively, from 7 to 17 hours for FE model and atlas creation [16]. However, intra-operative steps, when the atlas-based method is utilized for estimation, need 11-13 minutes to be performed [16]. As a result, if ACKF is more accurate and requires less computational time than the atlas-based method, it is preferable to be used for updating brain images. Moreover, since the intra-operative steps do not need much time to be done, it is possible to update the images several times during surgery and minimize the effect of brain shift.

The computed $\hat{\alpha}$ minimizes (8), however it is needed to investigate \hat{x}_{ACKF} as well; therefore, the following theorem, in this regard, is presented.

Theorem 1: Consider equations (2), (3), (4), (5), and the following general estimation of brain shift

$$\hat{x}_H = \bar{x} + H(y - C\bar{x}) \quad (12)$$

where \hat{x}_H is the $n \times 1$ vector estimation of x for a gain matrix H , to be determined. If the covariance of b is unknown and the estimation error is defined as

$$e_H = x - \hat{x}_H \quad (13)$$

then

- I) The obtained estimation by ACKF, (11), is the best unbiased estimation that minimizes $\max(\text{Var}(e_H))$,
- II) ACKF employs an estimation of $\text{Cov}(x)$ that results the best covariance estimation error bounds.

Proof: *Part I)* The proof of this part is inspired from [13]. To show that the estimation is unbiased, one needs to substitute (3) in (12) and compute $E[e_H]$, then it can be seen that $E[e_H] = 0$.

The covariance of e_H can be obtained by using (3), (4), (12), and (13) as follows:

$$\text{Cov}(e_H) = (I - HC) M \text{Cov}(\alpha) M^T (I - HC)^T. \quad (14)$$

Because it is assumed that the covariance of b is unknown, $\text{Cov}(\alpha)$ should be expressed in terms of that. Towards this end, the relationship between α and b can be obtained by employing (2) and (4) as follows:

$$KM\alpha = b. \quad (15)$$

By pre-multiplying $M^T K^T$ in (15) and inverting $M^T K^T K M$, we can get

$$\alpha = (M^T K^T K M)^{-1} M^T K^T b.$$

It is obvious that a similar relationship should hold between $\bar{\alpha}$ and \bar{b} ; thus, one can get

$$\text{Cov}(\alpha) = W Q W^T \quad (16)$$

$$W := (M^T K^T K M)^{-1} M^T K^T \quad (17)$$

where $Q = Q^T > 0$ is the covariance of b which is unknown. By substituting (16) in (14), one can get

$$\text{Cov}(e_H) = (I - HC) M W Q W^T M^T (I - HC)^T. \quad (18)$$

The trace of (18) is the variance of e_H , given as

$$\text{Var}(e_H) = \text{Tr}\{\text{Cov}(e_H)\}. \quad (19)$$

By utilizing the following row form

$$(I - HC) M W = \begin{bmatrix} h_1^T \\ h_2^T \\ \vdots \\ h_n^T \end{bmatrix} \quad (20)$$

together with equations (18) and (19), we can write

$$\text{Var}(e_H) = \sum_{i=1}^n h_i^T Q h_i. \quad (21)$$

Since Q is a symmetric positive definite matrix, the following inequality can be considered

$$\lambda_{\min}(Q) I \leq Q \leq \lambda_{\max}(Q) I. \quad (22)$$

Using (21) and (22), the resulting equation is as follows:

$$\lambda_{\min}(Q) \sum_{i=1}^n h_i^T h_i \leq \text{Var}(e_H) \leq \lambda_{\max}(Q) \sum_{i=1}^n h_i^T h_i. \quad (23)$$

According to *Minimax Theory* [31], the gain matrix H should minimize the maximum of $\text{Var}(e_H)$. Therefore, by employing (20) and (23), the following cost function can be considered

$$J_{\text{Var}} = \text{Tr}\{(I - HC) M W W^T M^T (I - HC)^T\}.$$

By calculating $\frac{\partial J_{\text{Var}}}{\partial H} = 0$ and utilizing (17), one can get

$$H = M (M^T K^T K M)^{-1} M^T C^T \times (C M (M^T K^T K M)^{-1} M^T C^T)^{-1}. \quad (24)$$

By using H and (12), one can see that \hat{x}_H is equal to ACKF estimation.

Part II) The best estimation of brain shift, \hat{x}_B , that has the smallest estimation error covariance, can be obtained from minimization of the following cost function over \hat{x}_B [32]:

$$J = E[(x - \hat{x}_B)^T \Sigma^{-1} (x - \hat{x}_B)] + 2\lambda^T (y - C\hat{x}_B)$$

where Σ is the covariance of x . The solution to this optimization problem is given as [32]:

$$\hat{x}_B = \bar{x} + \Sigma C^T (C \Sigma C^T)^{-1} (y - C\bar{x}). \quad (25)$$

It is assumed that $\text{Cov}(\mathbf{b})$ is unknown; thus, Σ is also unknown and we need to estimate it. By employing (4), (16), and (17) one can get

$$\Sigma = M(M^T K^T K M)^{-1} M^T K^T Q K M \times (M^T K^T K M)^{-1} M^T.$$

If the estimation of Σ is considered as $\hat{\Sigma}$, we can consider the covariance estimation error, $\tilde{\Sigma}$, as follows:

$$\tilde{\Sigma} = M(M^T K^T K M)^{-1} M^T K^T Q \times K M (M^T K^T K M)^{-1} M^T - \hat{\Sigma}. \quad (26)$$

By employing (22) and (26), one can get

$$\lambda_{\min}(\mathbf{Q})M(M^T K^T K M)^{-1} M^T - \hat{\Sigma} \leq \tilde{\Sigma} \leq \lambda_{\max}(\mathbf{Q})M(M^T K^T K M)^{-1} M^T - \hat{\Sigma}. \quad (27)$$

Therefore, the estimation of Σ , that provides the best covariance estimation error bounds, is

$$\hat{\Sigma} = \rho M(M^T K^T K M)^{-1} M^T \quad (28)$$

where $\rho = \frac{\lambda_{\min}(\mathbf{Q}) + \lambda_{\max}(\mathbf{Q})}{2}$. Since the eigenvalues of \mathbf{Q} are unknown, ρ is also unknown. Nevertheless, one can consider any nonzero value for ρ , and that is because by substituting $\hat{\Sigma}$ obtained from (28) as the estimation of Σ in (25), the resulting equation for any nonzero ρ is equal to that of ACKF. In other words, for the best estimation of Σ , the resulting estimation obtained by (25) is equal to that of ACKF which completes the proof. \square

One may assume that employing a recursive form of (11) could improve the accuracy of estimation. To investigate that, the following equation can be considered

$$\hat{\mathbf{x}}_i[k+1] = \hat{\mathbf{x}}_i[k] + M(M^T K^T K M)^{-1} M^T C^T \times (C M (M^T K^T K M)^{-1} M^T C^T)^{-1} (\mathbf{y} - C \hat{\mathbf{x}}_i[k])$$

where $\hat{\mathbf{x}}_i[0] = \bar{\mathbf{x}}$ and $k = 0, 1, \dots$. From (11) and the previous equation, one can see that $\hat{\mathbf{x}}_i[1] = \hat{\mathbf{x}}_{\text{ACKF}}$ and $\mathbf{y} = C \hat{\mathbf{x}}_{\text{ACKF}}$. Therefore, the second term on the right-hand side of the preceding equation is equal to zero for $k \geq 1$, and it can be easily shown by induction that $\hat{\mathbf{x}}_i[k+1] = \hat{\mathbf{x}}_i[1] = \hat{\mathbf{x}}_{\text{ACKF}}$ for all $k \geq 0$. Hence, the preceding recursive equation does not result in the improvement of accuracy, and using (11) is adequate for estimating brain shift. In addition, it is worth noting that other recursive forms of (11) do not affect the accuracy, but have an impact on the computational time of estimation. On the other hand, as it is explained in the next sections and validated by simulation results, ACKF is quite fast; hence, it does not require a recursive modification.

Considering the presented Theorem 1, ACKF is the best linear minimax estimator for brain shift when the covariance of \mathbf{b} is unknown and the atlas of brain deformations is employed. In [13], it is also shown that CKF is the best linear minimax estimator for brain shift when the covariance of \mathbf{b} is unknown. It is needed to compare ACKF with CKF method and see whether ACKF is more accurate.

Lemma 1: Consider equations (2), (3), (4), and (5). If ACKF estimation is given by (11) and CKF estimation, $\hat{\mathbf{x}}_{\text{CKF}}$,

is [13]:

$$\hat{\mathbf{x}}_{\text{CKF}} = \bar{\mathbf{x}} + K^{-1} K^{-T} C^T (C K^{-1} K^{-T} C^T)^{-1} (\mathbf{y} - C \bar{\mathbf{x}}) \quad (29)$$

then

- I) ACKF employs an estimation of $\text{Cov}(\mathbf{x})$ that has better covariance estimation error bounds,
- II) ACKF is a better minimax estimator of brain shift with lower maximum risk.

Proof: *Part I)* From (25) and (29), one can see that the utilized estimation of Σ in CKF, $\hat{\Sigma}_{\text{CKF}}$, can be considered as

$$\hat{\Sigma}_{\text{CKF}} = \rho K^{-1} K^{-T} \quad (30)$$

where ρ is a nonzero scalar. In CKF, the atlas of brain deformations is not employed; thus by using (2), the covariance of \mathbf{x} , Σ_{CKF} , can be considered as follows:

$$\Sigma_{\text{CKF}} = K^{-1} Q K^{-T}. \quad (31)$$

If the covariance estimation error of CKF, $\tilde{\Sigma}_{\text{CKF}}$, be defined as

$$\tilde{\Sigma}_{\text{CKF}} = \Sigma_{\text{CKF}} - \hat{\Sigma}_{\text{CKF}}$$

then by using (22), (30), and (31), one can get

$$(\lambda_{\min}(\mathbf{Q}) - \rho) K^{-1} K^{-T} \leq \tilde{\Sigma}_{\text{CKF}} \leq (\lambda_{\max}(\mathbf{Q}) - \rho) K^{-1} K^{-T}. \quad (32)$$

On the other hand, from Theorem 1, it can be seen that the covariance estimation of ACKF, $\hat{\Sigma}_{\text{ACKF}}$, is equal to $\hat{\Sigma}$ obtained from (28). Hence, the following inequality can be considered by substituting (28) into (27)

$$(\lambda_{\min}(\mathbf{Q}) - \rho) M(M^T K^T K M)^{-1} M^T \leq \tilde{\Sigma}_{\text{ACKF}} \leq (\lambda_{\max}(\mathbf{Q}) - \rho) M(M^T K^T K M)^{-1} M^T \quad (33)$$

where $\tilde{\Sigma}_{\text{ACKF}}$ is the covariance estimation error of ACKF. As can be seen, the scalars $\lambda_{\min}(\mathbf{Q}) - \rho$ and $\lambda_{\max}(\mathbf{Q}) - \rho$ are common in (32) and (33); thus, in order to compare $\tilde{\Sigma}_{\text{CKF}}$ and $\tilde{\Sigma}_{\text{ACKF}}$, we need to analyze the following equation

$$U := K^{-1} K^{-T} - M(M^T K^T K M)^{-1} M^T. \quad (34)$$

If the matrix $U \geq 0$, then it can be concluded that $\hat{\Sigma}_{\text{ACKF}}$ has better estimation error bounds than $\hat{\Sigma}_{\text{CKF}}$. Towards this end, one can pre- and post-multiply (34) by K and K^T , respectively, and get

$$K U K^T = I - K M (M^T K^T K M)^{-1} M^T K^T. \quad (35)$$

In order to show that $U \geq 0$, one needs to show that $K U K^T \geq 0$. By computing $K U K^T (K U K^T)^T$, which is a positive semi definite matrix, we can see that

$$K U K^T (K U K^T)^T = I - K M (M^T K^T K M)^{-1} M^T K^T. \quad (36)$$

Therefore, by employing (35) and (36), it can be concluded that $K U K^T \geq 0$.

Part II) If the estimation error of ACKF, e_{ACKF} , is defined as $e_{\text{ACKF}} = \mathbf{x} - \hat{\mathbf{x}}_{\text{ACKF}}$, then by utilizing (17), (20), (23), and (24), the following inequality can be obtained

$$\lambda_{\min}(\mathbf{Q}) \delta_{\text{ACKF}} \leq \text{Var}(e_{\text{ACKF}}) \leq \lambda_{\max}(\mathbf{Q}) \delta_{\text{ACKF}}$$

where

$$\delta_{\text{ACKF}} = \text{Tr} \{ \mathbf{R} - \mathbf{R} \mathbf{C}^T (\mathbf{C} \mathbf{R} \mathbf{C}^T)^{-1} \mathbf{C} \mathbf{R} \} \quad (37)$$

$$\mathbf{R} := \mathbf{M} (\mathbf{M}^T \mathbf{K}^T \mathbf{K} \mathbf{M})^{-1} \mathbf{M}^T. \quad (38)$$

For the estimation error of CKF, e_{CKF} , one can consider the following inequality in a similar way

$$\lambda_{\min}(\mathbf{Q}) \delta_{\text{CKF}} \leq \text{Var}(e_{\text{CKF}}) \leq \lambda_{\max}(\mathbf{Q}) \delta_{\text{CKF}}$$

where $e_{\text{CKF}} = \mathbf{x} - \hat{\mathbf{x}}_{\text{CKF}}$ and

$$\delta_{\text{CKF}} = \text{Tr} \{ \mathbf{P} - \mathbf{P} \mathbf{C}^T (\mathbf{C} \mathbf{P} \mathbf{C}^T)^{-1} \mathbf{C} \mathbf{P} \} \quad (39)$$

$$\mathbf{P} := \mathbf{K}^{-1} \mathbf{K}^{-T}. \quad (40)$$

Since ACKF and CKF are minimax estimators, it is required to compare their maximum risks to determine which one is more accurate [33]. Consequently, in order to show that ACKF is more accurate than CKF, it is needed to show that

$$\delta_{\text{ACKF}} \leq \delta_{\text{CKF}}. \quad (41)$$

Define \mathbf{V} as

$$\begin{aligned} \mathbf{V} := & \mathbf{P} - \mathbf{P} \mathbf{C}^T (\mathbf{C} \mathbf{P} \mathbf{C}^T)^{-1} \mathbf{C} \mathbf{P} - \mathbf{R} \\ & + \mathbf{R} \mathbf{C}^T (\mathbf{C} \mathbf{R} \mathbf{C}^T)^{-1} \mathbf{C} \mathbf{R} \end{aligned} \quad (42)$$

then

$$\delta_{\text{CKF}} - \delta_{\text{ACKF}} = \text{Tr} \{ \mathbf{V} \}.$$

By using (38), (40), and (42), it can be seen that $\mathbf{V} = \mathbf{V}^T$. Thus if $\mathbf{V} \geq 0$, all eigenvalues of \mathbf{V} are non-negative. On the other hand, we have

$$\text{Tr} \{ \mathbf{V} \} = \sum_{i=1}^n \lambda_i(\mathbf{V})$$

where $\lambda_i(\mathbf{V})$ is the i -th eigenvalue of \mathbf{V} . Therefore, to show (41), it is sufficient to show that $\mathbf{V} \geq 0$. By pre- and post-multiplying \mathbf{V} by \mathbf{K} and \mathbf{K}^T and using (38) and (40), one can compute $\mathbf{K} \mathbf{V} \mathbf{K}^T$ ($\mathbf{K} \mathbf{V} \mathbf{K}^T$) and get

$$\mathbf{K} \mathbf{V} \mathbf{K}^T (\mathbf{K} \mathbf{V} \mathbf{K}^T) = \mathbf{K} \mathbf{V} \mathbf{K}^T.$$

Hence $\mathbf{K} \mathbf{V} \mathbf{K}^T \geq 0$, which indicates that $\mathbf{V} \geq 0$. \square

Lemma 1 states that ACKF is better than CKF in terms of accuracy. It is worth to mention that ACKF is faster than CKF as well because unlike CKF, it does not directly depend on the inverse of \mathbf{K} , which in practice is a very large matrix.

As shown in Lemma 1, ACKF is more accurate than CKF since it utilizes the atlas of brain deformations. Nevertheless, both ACKF and CKF employ the same computation method, constrained Kalman filter, thus it can be concluded that utilization of the atlas results in a better estimation. Another method which uses the atlas of brain deformations is atlas-based method, however it employs a different computational method in comparison with ACKF. The following lemma is presented to compare these two methods, ACKF and atlas-based method, in terms of accuracy.

Lemma 2: Consider equations (2), (3), (4), and (5). If ACKF estimation is given by (11) and the estimation of atlas-based method, $\hat{\mathbf{x}}_{\mathbf{A}}$, is obtained as [15]:

$$\hat{\mathbf{x}}_{\mathbf{A}} = \mathbf{M} \hat{\boldsymbol{\alpha}}_{\mathbf{A}} \quad (43)$$

where $\hat{\boldsymbol{\alpha}}_{\mathbf{A}}$ is the solution of the following constrained optimization problem [15]:

$$\begin{aligned} \arg \min_{\hat{\boldsymbol{\alpha}}_{\mathbf{A}}} & (\mathbf{C} \mathbf{M} \hat{\boldsymbol{\alpha}}_{\mathbf{A}} - \mathbf{y})^T (\mathbf{C} \mathbf{M} \hat{\boldsymbol{\alpha}}_{\mathbf{A}} - \mathbf{y}) \\ \text{subject to} & \hat{\alpha}_{A_i} \geq 0, \sum_{i=1}^l \hat{\alpha}_{A_i} \leq 1 \end{aligned} \quad (44)$$

then ACKF results in a more accurate estimation of brain shift.

Proof: As can be seen from the constraints in (44), the feasible region is a subset of the following bound constraint

$$0 \leq \hat{\alpha}_{A_i} \leq 1. \quad (45)$$

The bound constraint can be written in a quadratic form as follows [34]:

$$(\hat{\alpha}_{A_i} - \hat{\alpha}'_{A_i})^2 \leq \sigma_i^2 \quad (46)$$

where $\hat{\alpha}'_{A_i} = \frac{1}{2}$ and $\sigma_i = \frac{1}{2}$. Since (46) circumscribes an ellipsoid around (45), the feasible region is also a subset of (46). Therefore, the following optimization problem can be considered

$$\begin{aligned} \arg \min_{\hat{\boldsymbol{\alpha}}_{\mathbf{A}}} & (\mathbf{C} \mathbf{M} \hat{\boldsymbol{\alpha}}_{\mathbf{A}} - \mathbf{y})^T (\mathbf{C} \mathbf{M} \hat{\boldsymbol{\alpha}}_{\mathbf{A}} - \mathbf{y}) \\ \text{subject to} & (\hat{\alpha}_{A_i} - \hat{\alpha}'_{A_i})^2 \leq \sigma_i^2. \end{aligned} \quad (47)$$

In [34], an algorithm is presented to find the solution of (47) identical to (44). The algorithm employs the penalty or weighted approach to find the solution from minimization of the following objective function

$$\begin{aligned} J_{\mathbf{A}} = & (\mathbf{C} \mathbf{M} \hat{\boldsymbol{\alpha}}_{\mathbf{A}} - \mathbf{y})^T (\mathbf{C} \mathbf{M} \hat{\boldsymbol{\alpha}}_{\mathbf{A}} - \mathbf{y}) \\ & + (\hat{\boldsymbol{\alpha}}_{\mathbf{A}} - \hat{\boldsymbol{\alpha}}'_{\mathbf{A}})^T \mathbf{D}_{\epsilon}^{-1} (\hat{\boldsymbol{\alpha}}_{\mathbf{A}} - \hat{\boldsymbol{\alpha}}'_{\mathbf{A}}), \end{aligned} \quad (48)$$

where

$$\begin{aligned} \mathbf{D}_{\epsilon} & := \epsilon \mathbf{D} \\ \mathbf{D} & := \text{diag}(\sigma_i^2), \end{aligned}$$

and ϵ is the penalty parameter that sets the radius of the ellipsoid. Minimization of (48) results the following equation [34]:

$$\hat{\boldsymbol{\alpha}}_{\mathbf{A}} = \hat{\boldsymbol{\alpha}}'_{\mathbf{A}} + (\mathbf{M}^T \mathbf{C}^T \mathbf{C} \mathbf{M} + \mathbf{D}_{\epsilon}^{-1})^{-1} \mathbf{M}^T \mathbf{C}^T (\mathbf{y} - \mathbf{C} \mathbf{M} \hat{\boldsymbol{\alpha}}'_{\mathbf{A}}). \quad (49)$$

According to the algorithm, one should compute (49) for different amounts of ϵ to find the solution that satisfies the original constraints in (44). Let ϵ_1 be the amount of penalty parameter that solves the problem, then by using (43) we can have

$$\begin{aligned} \hat{\mathbf{x}}_{\mathbf{A}} = & \mathbf{M} \hat{\boldsymbol{\alpha}}'_{\mathbf{A}} \\ & + \mathbf{M} (\mathbf{M}^T \mathbf{C}^T \mathbf{C} \mathbf{M} + \mathbf{D}_{\epsilon_1}^{-1})^{-1} \mathbf{M}^T \mathbf{C}^T (\mathbf{y} - \mathbf{C} \mathbf{M} \hat{\boldsymbol{\alpha}}'_{\mathbf{A}}), \end{aligned} \quad (50)$$

where $\mathbf{D}_{\epsilon_1} = \epsilon_1 \mathbf{D}$. By comparing (50) with (12), one can see that if $\bar{\boldsymbol{\alpha}} = \hat{\boldsymbol{\alpha}}'_{\mathbf{A}}$, the estimation of atlas-based method is a special case of (12). Furthermore, as shown in Theorem 1, the best estimation for the general form (12) is ACKF. Hence ACKF is more accurate than the atlas-based method. \square

It is worth to mention that in practice, the computational time of ACKF is lower than atlas-based method, and it is because the optimization in atlas-based method is solved by numerical recursive methods.

III. SIMULATION

To test the fidelity of proposed approach, this section provides simulation of brain shift and results of its estimation. In this regard, brain shift is simulated using the governing equations of brain and its boundary conditions. Then, the brain shift is estimated using ACKF, CKF, and atlas-based method.

A. Brain Shift Simulation

To simulate brain shift, we need governing equations, geometry, and boundary conditions. The governing equations are (1), and the geometry of brain is considered as a sphere 22 cm in diameter [13], [35]. The boundary conditions consist of displacement, pressure, and force boundary conditions which are shown in Figure 2 and were first reported in [36]. Figure 2.a shows displacement boundary conditions in which the first region (white) represents the region under surgery and is stress free. The second region (light gray) which is in contact with the cranial wall, the interior wall of the skull, is a slip boundary condition. Therefore, it can move along the cranial wall, but movement in the normal direction is not permitted. The third region (dark gray) is associated with the brain stem and is fixed. Figure 2.b expresses pressure boundary conditions and consists of a region above (region 1) and a region below (region 2) the level of intra-operative CSF drainage; therefore, region 1 (gray) is exposed to atmospheric pressure and region 2 (white) is a non-draining surface. The plane of intra-operative CSF drainage, which is the boundary between regions 1 and 2 in Figure 2.b, is perpendicular to the direction of gravity which is the force boundary condition.

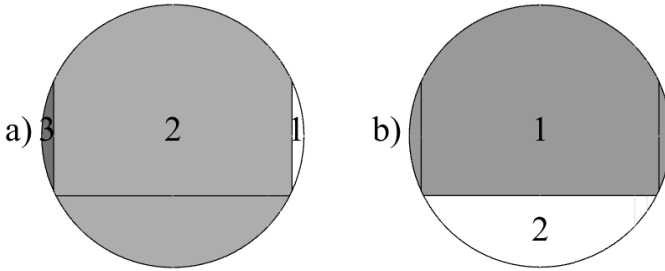


Fig. 2: Boundary conditions. a) Displacement Boundary conditions: Surface 1 is stress free. Surface 2 moves along the skull. Surface 3 is fixed. b) Pressure boundary conditions: Surface 1 is at atmospheric pressure. Surface 2 allows no fluid drainage.

To simulate brain shift, the model is solved by *COMSOL Multiphysics* on a computer with Intel Quad Core i5 with 4 GB of ram running Windows 7 64 bit, and the result is depicted in Figure 3. It can be seen that the brain is deformed, which in practice degrades the accuracy of neuronavigation systems. Also, the largest brain shift has occurred on the exposed brain surface which is a result of opening the dura and gravity. In the next section, the brain shift is estimated using ACKF and compared to the estimation of other methods.

B. Brain Shift Estimation

In order to estimate brain shift, as shown in Figure 1, it is required to perform pre- and intra-operative steps. The

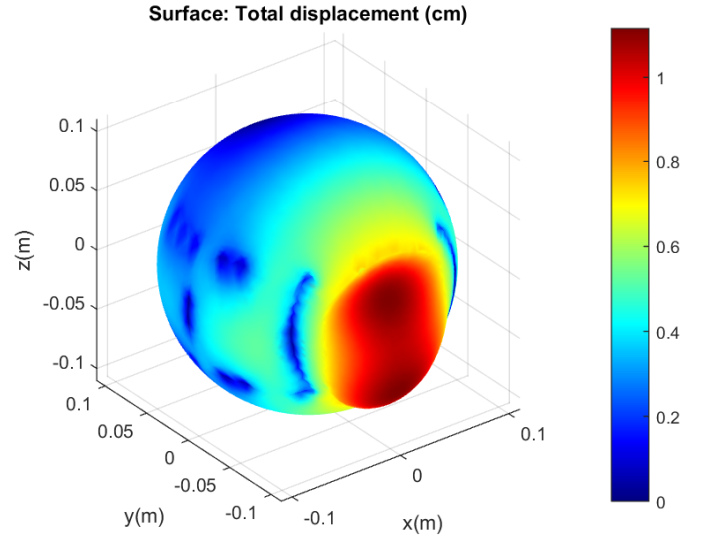


Fig. 3: Result of brain shift simulation.

next two sections explain these steps which are done in this simulation.

1) *Pre-operative Phase*: The considered geometry of brain, i.e., a sphere 22 cm in diameter, and the brain model (1) are employed for constructing the FE model of brain. Then, using an approximation of craniotomy size and head orientation, twelve nodes on the brain surface are used for obtaining the output model (3). It is assumed that during surgery, these nodes are located on the exposed brain surface and their deformation can be captured using intra-operative brain surface imaging. On the other hand, an important pre-operative step in the proposed estimation method is the process of atlas creation to ensure that the range of possible boundary conditions are employed to make the atlas M . To construct the atlas, three craniotomy sizes, three CSF drainage levels, and 65 orientations are employed, resulting in 585 displacement data sets for the atlas. It should be mentioned that utilized boundary conditions in the simulation of brain shift are not part of the atlas. Furthermore, to investigate the performance and robustness of the proposed method, it is needed to analyze the obtained brain shift estimation for atlas with perturbed displacement data [12]. Towards this end, 5% white Gaussian noise is added to the atlas for building a perturbed set of brain deformations. In addition, similar to [13], the initial brain shift estimation is considered equal to zero, i.e. $\bar{x} = 0$.

2) *Intra-operative Phase*: It is assumed that the deformation of considered twelve nodes on the exposed brain surface are obtained intra-operatively. Then, these sparse measurements are used for estimating the brain shift.

C. Simulation Results

By employing the created atlas and sparse measurements from the previous section, ACKF resulted an estimation of brain shift which is shown in Figure 4.

By comparing Figures 3 and 4, it seems that ACKF has resulted an estimation close to the actual brain shift. However, these figures merely represent surface brain shift and its

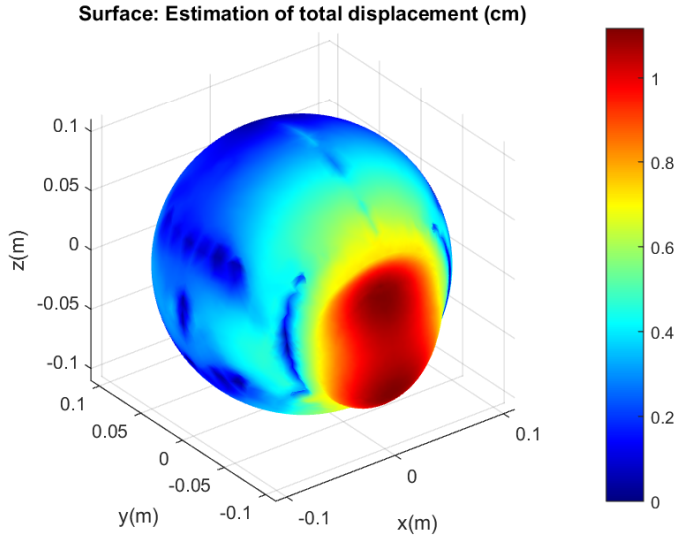


Fig. 4: Result of ACKF brain shift estimation.

estimation, and to perform a more detailed comparison, it is required to compare and evaluate sub-surface brain shift estimation. Therefore, the vectors \boldsymbol{x} and $\hat{\boldsymbol{x}}_{\text{ACKF}}$ are depicted in Figure 5 to express brain shift and its estimation for the entire sphere. It can be easily seen that the obtained brain shift estimation is also accurate for sub-surface tissues, and in turn, it can be used for improving pre-operative brain images.

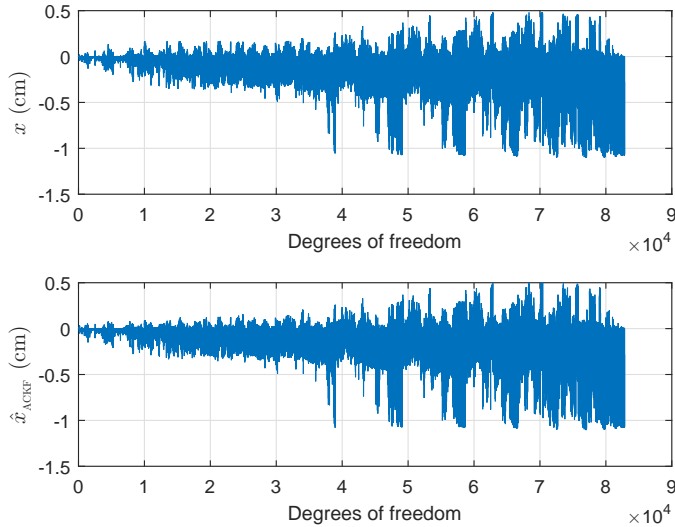


Fig. 5: Brain shift vector \boldsymbol{x} and its ACKF estimation $\hat{\boldsymbol{x}}_{\text{ACKF}}$.

In order to validate Lemmas 1 and 2, brain shift is also estimated using CKF and the atlas-based method, and their estimation errors together with ACKF are shown in Figure 6. The figure reveals that ACKF has resulted in a much better estimation in terms of maximum error. To summarize the performance of all three estimation methods, the computational cost and specifications of estimation errors in Figure 6 are reported in Table II. Table II presents computational time, norm of error, maximum absolute error, and mean of absolute error for the methods. It can be seen that ACKF is not only

able to compensate brain deformation more accurately, but also needs less intra-operative computation time. As shown in Lemmas 1 and 2, better accuracy is a result of using the atlas and constrained Kalman filter. Moreover, ACKF needs less computations since, unlike CKF, it does not need to compute the inverse of \boldsymbol{K} , which is a large matrix. In addition, unlike the atlas-based method, its solution is not obtained by recursive numerical methods.

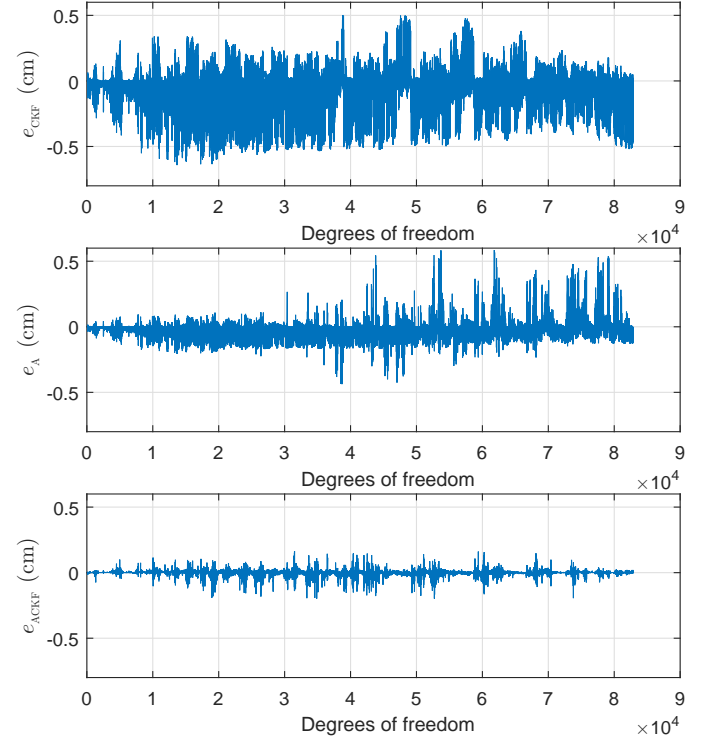


Fig. 6: Estimation error of CKF e_{CKF} , atlas-based method e_{A} , and ACKF e_{ACKF} .

TABLE II: Comparison over estimation error and intra-operative computational time of CKF, atlas-based method, and ACKF.

Method	t_{intra} (s)	$\text{norm}(e)$ (cm)	$\max(e)$ (cm)	$\text{mean}(e)$ (cm)
CKF	118.8	47.5	0.64	0.1
atlas-based	184.6	18.8	0.58	3.67×10^{-2}
ACKF	5.4	4.5	0.19	7.86×10^{-3}

In order to test the robustness of ACKF, the atlas with noise is utilized for obtaining estimations using the atlas-based method and ACKF, and the results are shown in Figure 7. It is obvious that even when the atlas is perturbed, ACKF provides preferable estimations. For a more detailed comparison, the specifications of the estimation errors and computational times are illustrated in Table III. The results show that as long as the actual brain shift is contained in the atlas, ACKF is relatively insensitive to noise. In other words, in order to obtain an accurate estimation, it is only required to exist an unknown vector $\boldsymbol{\alpha}$ that satisfies (4). Therefore, if appropriate boundary conditions are utilized for constructing the atlas, it can be

guaranteed that ACKF performs well and provides accurate estimations.

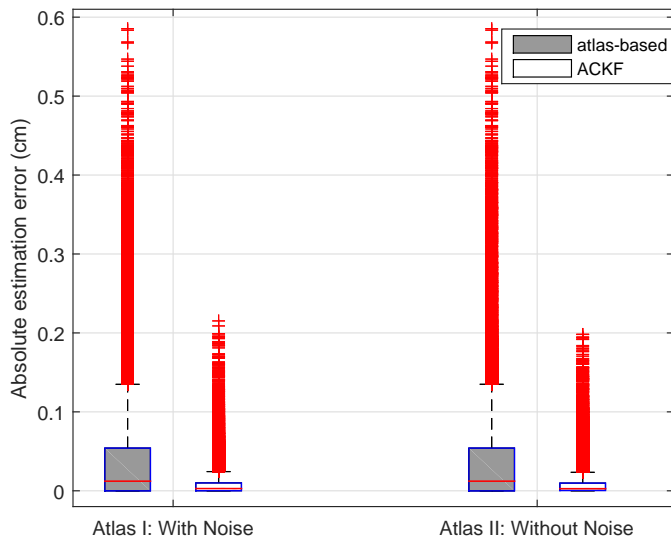


Fig. 7: Boxplot of absolute estimation error for atlas with and without noise.

TABLE III: Comparison over estimation error and intra-operative computational time of atlas-based method and ACKF for atlas with noise.

Method	t_{intra} (s)	$\text{norm}(e)$ (cm)	$\text{max}(e)$ (cm)	$\text{mean}(e)$ (cm)
atlas-based	194.6	18.8	0.58	3.67×10^{-2}
ACKF	5.5	4.7	0.21	8.04×10^{-3}

IV. CONCLUSIONS

In this paper, an estimation method based on Atlas of brain deformations and Constrained Kalman Filter (ACKF) was proposed to estimate brain shift intra-operatively. It was shown that ACKF results the best estimation when the covariance of boundary conditions of the brain model is unknown. Moreover, the proposed method was compared with two existing methods and it was demonstrated that consequences of employing ACKF is a more accurate estimation and less computational time which make the method suitable for the use in the operating room.

REFERENCES

- [1] Roberts DW, Hartov A, Kennedy FE, Miga MI, Paulsen KD. Intraoperative brain shift and deformation: a quantitative analysis of cortical displacement in 28 cases. *Neurosurgery* 1998; **43**(4):749–758.
- [2] Nimsky C, Ganslandt O, Hastreiter P, Fahlbusch R. Intraoperative compensation for brain shift. *Surgical neurology* 2001; **56**(6):357–364.
- [3] Wang MN, Song ZJ. Classification and analysis of the errors in neuronavigation. *Neurosurgery* 2011; **68**(4):1131–1143.
- [4] Loh PS, Vijayan R. Intraoperative magnetic resonance imaging. *Challenging Topics in Neuroanesthesia and Neurocritical Care*. Springer, 2017; 253–258.
- [5] Schichor C, Terpolilli N, Thorsteinsdottir J, Tonn JC. Intraoperative computed tomography in cranial neurosurgery. *Neurosurgery Clinics* 2017; **28**(4):595–602.

- [6] Morin F, Courtecuisse H, Reinertsen I, Le Lann F, Palombi O, Payan Y, Chabanas M. Brain-shift compensation using intraoperative ultrasound and constraint-based biomechanical simulation. *Medical Image Analysis* 2017; **40**(Supplement C):133–153.
- [7] Simpson AL, Dumpuri P, Ondrake JE, Weis JA, Jarnagin WR, Miga MI. Preliminary study of a novel method for conveying corrected image volumes in surgical navigation. *The International Journal of Medical Robotics and Computer Assisted Surgery* 2013; **9**(1):109–118.
- [8] Zhang C, Wang M, Song Z. A brain-deformation framework based on a linear elastic model and evaluation using clinical data. *IEEE Transactions on Biomedical Engineering* 2011; **58**(1):191–199.
- [9] Liu Y, Song Z. A robust brain deformation framework based on a finite element model in IGNS. *The International Journal of Medical Robotics and Computer Assisted Surgery* 2008; **4**(2):146–157.
- [10] Li P, Wang W, Song Z, An Y, Zhang C. A framework for correcting brain retraction based on an eXtended Finite Element Method using a laser range scanner. *International journal of computer assisted radiology and surgery* 2014; **9**(4):669–681.
- [11] Joldes GR, Wittek A, Miller K. An adaptive dynamic relaxation method for solving nonlinear finite element problems. application to brain shift estimation. *International journal for numerical methods in biomedical engineering* 2011; **27**(2):173–185.
- [12] Dumpuri P, Thompson RC, Dawant BM, Cao A, Miga MI. An atlas-based method to compensate for brain shift: Preliminary results. *Medical Image Analysis* 2007; **11**(2):128–145.
- [13] Shakarami M, Suratgar AA, Talebi HA. Estimation of intra-operative brain shift based on constrained Kalman filter. *ISA transactions* 2015; **55**:260–266.
- [14] Dumpuri P, Thompson RC, Cao A, Ding S, Garg I, Dawant BM, Miga M, *et al.* A fast and efficient method to compensate for brain shift for tumor resection therapies measured between preoperative and postoperative tomograms. *IEEE Transactions on Biomedical Engineering* 2010; **57**(6):1285–1296.
- [15] Chen I, Coffey AM, Ding S, Dumpuri P, Dawant BM, Thompson RC, Miga M, *et al.* Intraoperative brain shift compensation: accounting for dural septa. *IEEE Transactions on Biomedical Engineering* 2011; **58**(3):499–508.
- [16] Sun K, Pheiffer TS, Simpson AL, Weis J, Thompson RC, Miga M, *et al.* Near real-time computer assisted surgery for brain shift correction using biomechanical models. *IEEE Journal of Translational Engineering in Health and Medicine* 2014; **2**:1–13.
- [17] Miga MI, Sun K, Chen I, Clements LW, Pheiffer TS, Simpson AL, Thompson RC. Clinical evaluation of a model-updated image-guidance approach to brain shift compensation: experience in 16 cases. *International journal of computer assisted radiology and surgery* 2016; **11**(8):1467–1474.
- [18] Zanni L, Le Boudec JY, Cherkaoui R, Paolone M. A prediction-error covariance estimator for adaptive Kalman filtering in step-varying processes: Application to power-system state estimation. *IEEE Transactions on Control Systems Technology* 2017; **25**(5):1683–1697.
- [19] Zhang Y, Xu Q. Adaptive sliding mode control with parameter estimation and Kalman filter for precision motion control of a piezo-driven microgripper. *IEEE Transactions on Control Systems Technology* 2017; **25**(2):728–735.
- [20] Simon D. Kalman filtering with state constraints: a survey of linear and nonlinear algorithms. *IET Control Theory and Applications* 2010; **4**(8):1303–1318.
- [21] Bayat M, Crasta N, Aguiar AP, Pascoal AM. Range-based underwater vehicle localization in the presence of unknown ocean currents: Theory and experiments. *IEEE Transactions on control systems technology* 2016; **24**(1):122–139.
- [22] Biot MA. General theory of three-dimensional consolidation. *Journal of applied physics* 1941; **12**(2):155–164.
- [23] Paulsen KD, Miga M, Kennedy FE, Hoopens P, Hartov A, Roberts DW, *et al.* A computational model for tracking subsurface tissue deformation during stereotactic neurosurgery. *IEEE Transactions on Biomedical Engineering* 1999; **46**(2):213–225.
- [24] Ji S, Hartov A, Roberts D, Paulsen K. Data assimilation using a gradient descent method for estimation of intraoperative brain deformation. *Medical image analysis* 2009; **13**(5):744–756.
- [25] Miga MI, Paulsen KD, Lemery JM, Eisner SD, Hartov A, Kennedy FE, Roberts DW. Model-updated image guidance: initial clinical experiences with gravity-induced brain deformation. *IEEE Transactions on Medical Imaging* 1999; **18**(10):866–874.
- [26] Warfield SK, Talos F, Tei A, Bharatha A, Nabavi A, Ferrant M, Black PM, Jolesz FA, Kikinis R. Real-time registration of volumetric brain

- mri by biomechanical simulation of deformation during image guided neurosurgery. *Computing and Visualization in Science* 2002; **5**(1):3–11.
- [27] Narasimhan S, Weis JA, Godage IS, Webster R, Weaver K, Miga MI. Development of a mechanics-based model of brain deformations during intracerebral hemorrhage evacuation. *Proc. of SPIE*, vol. 10135, 2017; 1–12.
- [28] Lynch DR. *Numerical partial differential equations for environmental scientists and engineers: a first practical course*. US: Springer, 2005.
- [29] Lunn KE, Paulsen KD, Lynch DR, Roberts DW, Kennedy FE, Hartov A. Assimilating intraoperative data with brain shift modeling using the adjoint equations. *Medical image analysis* 2005; **9**(3):281–293.
- [30] Tikhonov AN. Regularization of incorrectly posed problems. *SOVIET MATHEMATICS DOKLADY*, 1963.
- [31] Norton JP. *An introduction to identification*. New York: Academic Press, 1986.
- [32] Simon D. *Optimal state estimation: Kalman, H infinity, and nonlinear approaches*. New York: Wiley, 2006.
- [33] Wasserman L. *All of statistics: a concise course in statistical inference*. Springer Science & Business Media, 2013.
- [34] Mead JL, Renaut RA. Least squares problems with inequality constraints as quadratic constraints. *Linear Algebra and its Applications* 2010; **432**(8):1936–1949.
- [35] Hamidian H, Soltanian-Zadeh H, Faraji-Dana R, Gity M. Estimating brain deformation during surgery using finite element method: optimization and comparison of two linear models. *Journal of Signal Processing Systems* 2009; **55**(1-3):157–167.
- [36] Miga M, Paulsen K, Kennedy F, Hoopes J, Hartov A, Roberts D. Initial in-vivo analysis of 3d heterogeneous brain computations for model-updated image-guided neurosurgery. *Medical Image Computing and Computer-Assisted Intervention–MICCAI98*. Berlin: Springer, 1998; 743–752.



Heidar A. Talebi (M'02–SM'08) received the B.Sc. degree in electrical engineering from Ferdowsi University, Mashhad, Iran, in 1988, the M.Sc. degree in electrical engineering from Tarbiat Modarres University, Tehran, Iran, in 1991, and the Ph.D. degree in electrical engineering from Concordia University, Montreal, QC, Canada, in 1997.

He was a Postdoctoral Fellow and a Research Fellow at Concordia University and The University of Western Ontario. In 1999, he joined Amirkabir University of Technology, Tehran, Iran. He is currently a professor in the Department of Electrical Engineering, and his research interests include control, robotics, medical robotics, fault diagnosis and recovery, intelligent systems, adaptive control, nonlinear control, and real-time systems.



Mehran Shakarami received the M.Sc. degree in electrical engineering from Amirkabir University of Technology (Tehran polytechnic), Tehran, Iran, in 2014, and B.Sc. and A.Sc. degrees from Shamsipour College, Tehran, Iran, in 2011 and 2009, respectively. His current research interests include linear and nonlinear control, adaptive control, robust control, system identification, and estimation.



Amir Abolfazl Suratgar (M'09–SM'14) received his B.S. degree in electrical engineering from Isfahan University of technology, Isfahan, Iran, in 1996. He was honored M.S. and Ph.D. degrees in control engineering from Amirkabir University of Technology (Tehran polytechnic), Tehran, Iran, in 1999 and 2002, respectively. Currently, he is an Associate Professor in Amirkabir University of Technology (Tehran polytechnic), Tehran, Iran. The areas of his research interests are optimal control and optimization, computational intelligence, neuroscience. He

has published more than 140 papers in scientific journals and conferences.